Hemodynamic Assessment of Celiaco-mesenteric Anastomosis in Patients with Pancreaticoduodenal Artery Aneurysm Concomitant with Celiac Artery Occlusion using Flow-sensitive Four-dimensional Magnetic Resonance Imaging

Y. Mano [a], Y. Takehara [b], T. Sakaguchi [a], M.T. Alley [c], H. Isoda [d], T. Shimizu [e], T. Wakayama [f], M. Sugiyama [b], H. Sakahara [b], H. Konno [a], N. Unno [a,*]

[a] Second Department of Surgery, Hamamatsu University School of Medicine, Hamamatsu, Japan
[b] Department of Radiology, Hamamatsu University School of Medicine, Hamamatsu, Japan
[c] Department of Radiology, Stanford University, Palo Alto, CA, USA
[d] Department of Radiological Sciences, Department of Radiological and Medical Laboratory Sciences, Nagoya University Graduate School of Medicine, Nagoya, Japan
[e] Renaissance Technology Corp., Hamamatsu, Japan
[f] GE Healthcare Japan, Hino, Japan

WHAT THIS PAPER ADDS

Pancreaticoduodenal arteries (PDA) aneurysms are rare; however, PDA aneurysms are among the most life-threatening of all splanchnic aneurysms. Fifty to eighty percent of PDA aneurysms are reported to accompany celiac artery stenosis. We assessed hemodynamic parameters such as flow volume, maximum flow velocity, wall shear stress, and oscillatory shear index using four-dimensional flow-sensitive magnetic resonance imaging (4D-Flow). 4D-Flow identified vortex flow and heterogenous distribution patterns of wall shear stress in not only PDA aneurysms but also across entire PDAs. Resected PDA aneurysms are all atherosclerotic. This study gained insights into the pathogenesis of PDA aneurysms.

Objectives: Many pancreaticoduodenal artery (PDA) aneurysms are associated with celiac artery (CA) stenosis. The pathogenesis of PDA aneurysm may be associated with hemodynamic changes due to CA stenosis/occlusion. The aim of this study was to assess the hemodynamic changes of celiaco-mesenteric anastomosis in patients with PDA aneurysms concomitant with CA occlusion using four-dimensional flow-sensitive magnetic resonance imaging (4D-Flow).

Methods: 4D-Flow was performed preoperatively on five patients. Seven age- and sex-matched individuals were used as controls. Hemodynamic parameters such as flow volume and maximum flow velocity in PDAs, gastroduodenal arteries, common hepatic arteries, and superior mesenteric arteries were compared between both groups. Wall shear stress (WSS) and oscillatory shear index (OSI) were mapped in both groups.

Results: In the patient group, 4D-Flow identified retrograde flow of both gastroduodenal arteries and common hepatic arteries. Heterogeneous distribution patterns of both WSS and OSI were identified across the entire PDA in the patient group. OSI mapping showed multiple regions with extremely high OSI values (OSI $>$ 0.3) in all patients. All PDA aneurysms, which were surgically resected, were atherosclerotic.

Conclusions: 4D-Flow identified hemodynamic changes in celiaco-mesenteric arteries in patients with PDA aneurysms with concomitant CA occlusion. These hemodynamic changes may be associated with PDA aneurysm formation.

Article history: Received 30 April 2013, Accepted 20 June 2013, Available online 21 July 2013

Keywords: 4D-Flow, Arteriosclerosis, Celiac artery, Oscillatory shear index, Pancreaticoduodenal artery aneurysm, Shear stress

INTRODUCTION

The pancreaticoduodenal arcades comprise the arterial network encircling the pancreatic head. These arcades connect the celiac artery (CA) system and the superior mesenteric artery via the superior and the inferior pancreaticoduodenal arteries (PDAs). Aneurysms at this arcade are often collectively described as PDA aneurysms. PDA

* Corresponding author. N. Unno, Division of Vascular Surgery, Hamamatsu University School of Medicine, 1-20-1 Handayama, Higashi-ku, Hamamatsu 431-3192, Japan.

E-mail address: unno@hama-med.ac.jp (N. Unno).

1078-5884/$ — see front matter © 2013 European Society for Vascular Surgery. Published by Elsevier Ltd. All rights reserved.

http://dx.doi.org/10.1016/j.ejvs.2013.06.011

aneurysms are unusual, and constitute only 2% of all visceral aneurysms.[1] However, PDA aneurysms are among the most life-threatening of all splanchnic aneurysms, with a mortality rate of up to 50% in case of a ruptured aneurysm.[1,2] Accumulating evidence reveals that 50–80% of PDA aneurysms are associated with CA stenosis.[2–4]

The purpose of this study was to assess hemodynamic alterations across the entire celiaco-mesenteric anastomosis, including the gastroduodenal artery (GDA), common hepatic artery (CHA), proper hepatic artery (PHA), and superior mesenteric artery (SMA), in patients with PDA aneurysms accompanied by CA occlusion. To gain insight into the mechanisms underlying PDA aneurysms, we used a four-dimensional (4D) flow-sensitive magnetic resonance imaging (MRI) device (4D-Flow). 4D-Flow enables the study of arterial hemodynamics, flow patterns, and derived vessel wall parameters in vivo; it serves as an important tool for both diagnosis and preoperative evaluation.[5–7] In this article, the results of patients with PDA aneurysms are compared with those of age- and sex-matched normotensive control participants with a normal aortic diameter and regular valve function.

MATERIALS AND METHODS

Subjects

This study was approved by the institutional review board of the University School of Medicine, Hamamatsu, Japan. Between August 2006 and November 2011, five consecutive patients with PDA aneurysm concomitant with CA occlusion underwent 4D-Flow to evaluate the hemodynamics of celiaco-mesenteric anastomosis. During the same period, seven individuals who did not have any cardiovascular or abdominal disease underwent 4D-Flow (control group). Written informed consent was obtained from all participants. All patients with PDA aneurysm were scheduled to undergo surgery, and 4D-Flow was performed preoperatively.

Time-resolved contrast-enhanced three-dimensional magnetic resonance angiography and 4D-Flow

Prior to 4D-Flow, contrast-enhanced three-dimensional magnetic resonance angiography was performed after bolus injection of gadolinium chelate with standard dose of 0.1 mmol/kg at an injection rate of 2–3 ml/s using an auto-injector. The contrast agent was used to increase the definition of the arterial wall boundary for post-processing and also to increase the signal-to-noise ratio in the 4D-Flow measurement.

Electrocardiography-gated, respiratory compensated three-dimensional (3D) fast spoiled gradient recalled echo-based 4D-Flow was conducted covering the PHA, PDA, proximal portion of SMA, and splenic artery with the parameters described in the Supplementary material (Supplementary method). 4D-Flow data sets and magnetic resonance angiography (MRA) data sets were transferred to a personal computer (Intel Core i7 CPU, 3.2 GHz, 12 GB RAM, Microsoft Windows 7) in DICOM format, and were post-processed with flow analysis software (Flova; Renaissance Technology, Hamamatsu, Japan). The application consisted of two processes of extraction and analysis. First, time-resolved images of 3D velocity vector fields were generated to overview the blood flow within the abdominal aorta. Then, 3D streamlines, wall shear stress (WSS) maps, and oscillatory shear index (OSI) maps were generated using 4D data sets (please refer to online-only supplementary material for further details on the method used).

Generation of 3D streamlines

We chose several cross-sectional planes every 2 cm traversing the abdominal aorta, CHA, GDA, PHA, SMA, and the first, second, and third segments of the pancreatic arcade. All planes were placed perpendicular to the longitudinal axis of the artery. We then generated 3D streamlines using the Runge–Kutta method.[8] 3D streamlines are integrated traces along the instantaneous velocity vector field that are color-coded according to the local velocity magnitude.

Calculation of WSS and OSI

WSS is defined as the product of fluid viscosity and shearing velocity of the neighboring vascular wall. The method we used to calculate the shearing velocity vector was similar to that reported by Masaryk et al.[9] and Cheng et al.;[10] however, our method was 3D not 2D. A 3D method to measure WSS has previously been reported by Isoda et al.,[11] on which our application is based. The dynamic viscosity of the blood was assumed to be 0.00384 Pa/s in the application.

OSI that reflects instantaneous fluctuation of WSS was calculated by temporal changes in the local WSS vector. OSI is defined as:

$$\left(1-\left|\int_T \mathrm{WSS}_i^t\,dt\right| \Big/ \int_T \left|\mathrm{WSS}_i^t\right| dt\right) \Big/ 2$$

where WSS_i^t is an instantaneous WSS vector.[12] OSI ranges from 0 to 0.5, and a large OSI implies that instantaneous WSS vectors fluctuate greatly in relation to the main stream direction at the calculated point during one cardiac cycle.

Flow dynamics of the arterial branches

The flow patterns in the PDA and other branches were evaluated by means of streamline observations by two

Table 1. Study population demographics.

	Control participants	Patients	*p*
Number, *n*	7	5	
Age, years [mean ± SD (median)]	62.5 ± 12.2 (65)	61.8 ± 15.6 (71)	0.664
Sex, *n* (male:female)	4:3	3:2	
Weight, kg (mean ± SD)	61.3 ± 11.8	62.8 ± 16.0	0.524
Height, cm (mean ± SD)	160.7 ± 6.9	160.6 ± 13.5	0.494

independent observers. To do that on a segment-by-segment basis, we classified the PDAs into three areas: arcade 1 (the portion near the SMA); arcade 2 (mid-portion of the PDA); arcade 3 (the portion near the GDA).

Statistical analysis

To detect statistically significant differences in demographics between patients and controls, a *t* test was used. For grading abnormal flow, flow volume, velocity, and WSS, the Mann–Whitney test was used. In all tests, $p < .05$ was considered significant. The reliability of two independent observers was assessed by Cohen's κ.[13] According to Landis and Koch,[14] $\kappa > 0.4$ indicates moderate reliability, whereas $\kappa > 0.6$, and $\kappa > 0.8$ indicate good and very good reliability, respectively. Prism v. 5.0 (graphPad Software Inc. La Jolla, Ca) was used for statistical analysis.

RESULTS

4D-Flow was performed in five patients with PDA aneurysm concomitant with CA occlusion. Among these five patients, four were hypertensive and three were smokers or had a history of smoking; none had hyperlipidemia or diabetes. For comparison purposes, we also analyzed seven volunteers who had neither CA occlusion nor PDA aneurysm. The

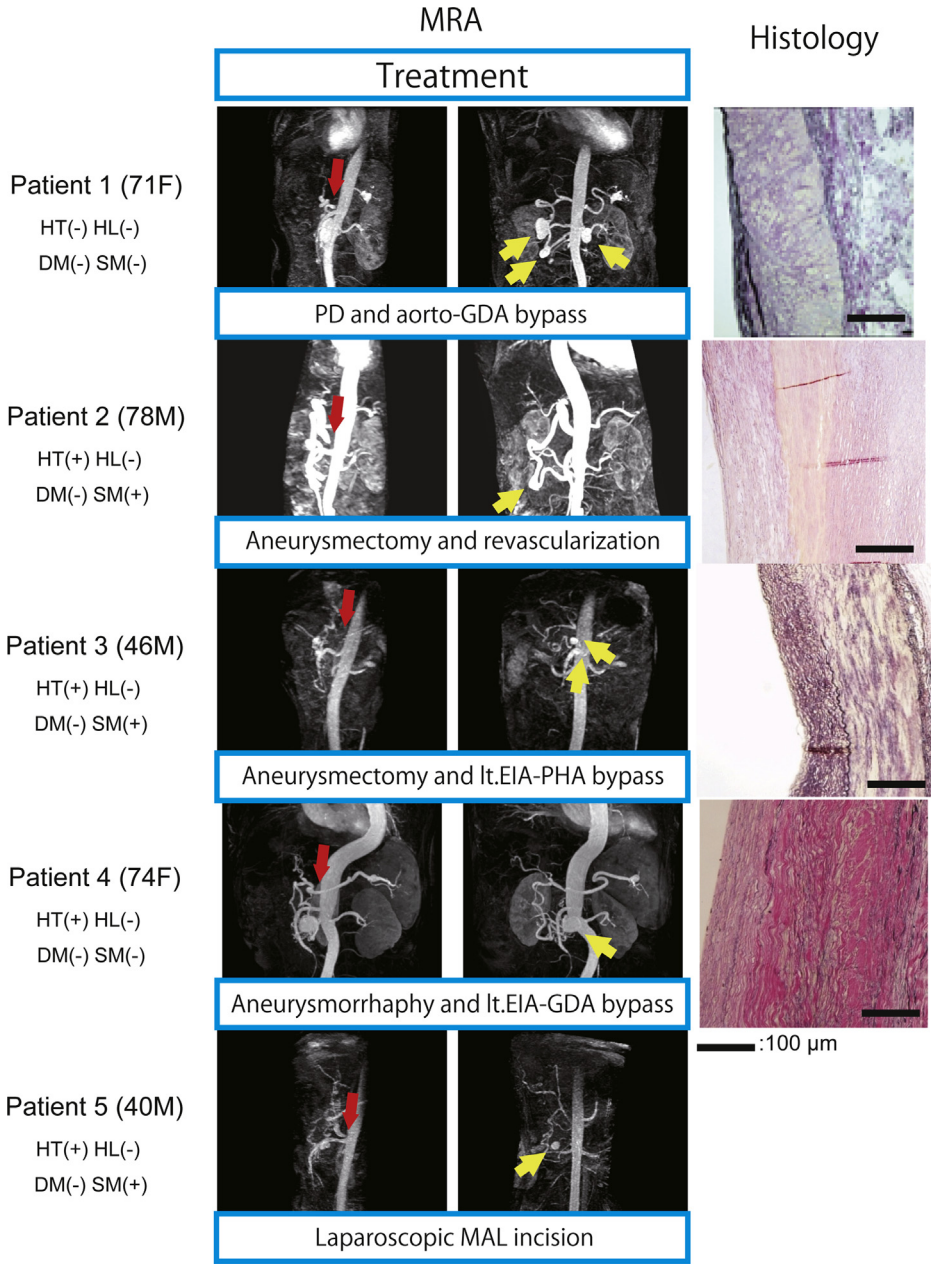

Figure 1. Preoperative magnetic resonance angiography (MRA; lateral and frontal view) and histological images of the resected pancreaticoduodenal artery (PDA) aneurysm (Elastica van Gieson staining) On MRA, red arrows indicate occlusion of the celiac artery; yellow arrows indicate PDA aneurysm. *Note*. 71F = 71-year-old female; HT = hypertension; HL = hyperlipidemia; DM = diabetes mellitus; SM = current or past history of smoking; 78M = 78-year-old male; 46M = 46-year-old male; 74F: 74-year-old female; GDA = gastroduodenal artery; lt.EIA = left external iliac artery; PHA = proper hepatic artery; MAL = median arcuate ligament.

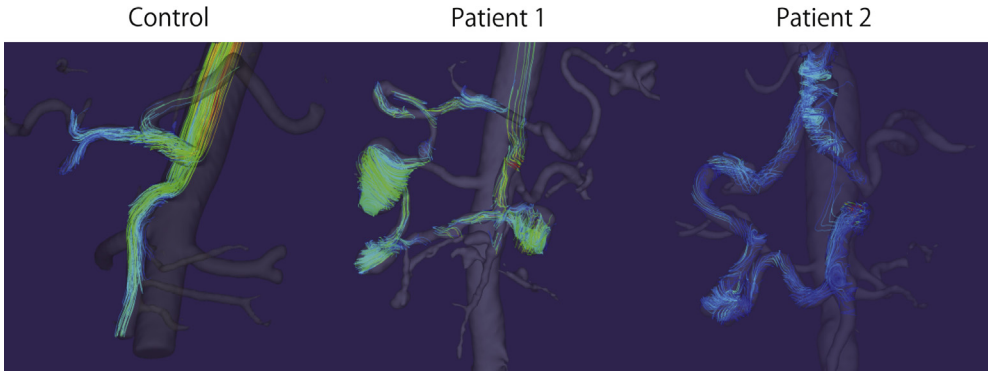

Figure 2. Three-dimensional visualization of blood streamline of systolic phase in a control participant, patient 1, and patient 2. *Note*. The line color indicates blood velocity, i.e., color changes from blue to red as the velocity increases. Blue indicates 0 mm/s; red indicates the maximum velocity in each case.

demographic data of both groups are summarized in Table 1.

MRAs are shown in Fig. 1. Patients 1 and 3 had multiple PDA aneurysms (patient 1 had more than 10 aneurysms, along with a splenic artery aneurysm, and patient 2 had two PDA aneurysms). The other three patients had a solitary PDA aneurysm. Before surgical treatment, all patients underwent 4D-Flow. With regard to treatment, patient 1 underwent pancreaticoduodenectomy with an aorto-GDA bypass for resection of the multiple aneurysms. Patients 2, 3, and 4 underwent aneurysmectomy with revascularization. Patient 5 underwent laparoscopic incision of the median arcuate ligament, according to the patient's request (with subsequent follow-up for the PDA). Histological examination revealed that all resected aneurysms in patients 1–4 were atherosclerotic (Fig. 1).

Streamline and flow pattern

Instantaneous 3D streamlines, instantaneous and time-averaged WSS distribution maps, and OSI distribution maps in arbitrary directions during the cardiac phase were obtained in both groups. Typical images of arterial streamline of a control participant and two patients (patients 1 and 2) are shown in Fig. 2 and in the Supplementary material (Supplementary Movies 1–3). In controls, the streamline in CA, CHA, PHA, GDA, and SMA was laminar and smooth. However, 4D-Flow did not allow visualization of the PDAs because of their relatively small size and low blood flow volume. However, in patients with PDA aneurysm, PDA aneurysms and PDA arteries were well visualized with 4D-Flow. Vortex or helical flow was observed throughout the entire PDA. Interestingly, CA, CHA, PHA, GDA, and SMA also showed vortex or helical flow in patients with PDA aneurysms, but not in control participants. Two independent observers evaluated the flow patterns in the PDA. Comparison of the flow grading revealed substantial interobserver agreement ($\kappa = 0.65$; agreement with vortex flow in the aorta, CHA, GDA, PHA, SMA, and in arcades 1–3). The flow grading and the frequency of vortex or helical flow in control participants and patients are summarized in Table 2. Vortex flow was not observed in the aorta of patients and control participants. However, in visceral arteries, such as the CHA, GDA, PHA, and SMA, vortex flow was more frequent in patients with PDA aneurysm than in controls. Vortex or helical flow was also frequently observed in arcades 1–3, but interobserver reliability was not calculated for these vessels because of lack of data in the control group.

Supplementary video related to this article can be found online at http://dx.doi.org/10.1016/j.ejvs.2013.06.011.

The following are the Supplementary video related to this article: Supplementary Movie 1: Three-dimensional visualization of blood streamline in a control participant. Supplementary Movie 2: Three-dimensional visualization of blood streamline in patient 1. Supplementary Movie 3: Three-dimensional visualization of blood streamline in patient 2.

WSS and OSI

Fig. 3 shows WSS in the aorta, CHA, GDA, PHA, SMA, and PDA. Patients with PDA aneurysms revealed more

Table 2. Abnormal flow pattern and frequency of vortex flow in control participants and patients.

	Control participants	Patients	*p*
Aorta	0 (0%)	0 (0%)	
CHA	0.50 ± 0.50 (50.0%)	1.0 ± 0.87 (62.5%)	0.09600
GDA	0.26 ± 0.45 (28.6%)	1.2 ± 0.87 (70.0%)	0.00580[a]
PHA	0.40 ± 0.49 (40.0%)	1.4 ± 0.80 (80.0%)	0.00500[a]
SMA	0.26 ± 0.45 (28.6%)	1.2 ± 0.60 (90.0%)	0.00082[a]
Arcade 1	N/A	0.80 ± 0.60 (70.0%)	
Arcade 2	N/A	0.70 ± 0.46 (70.0%)	
Arcade 3	N/A	0.60 ± 0.49 (60.0%)	
Aneurysm	N/A	1.75 ± 0.43 (100%)	

Note. All data are the mean ± SD of the two readers' scores.CHA = common hepatic arteries; GDA = gastroduodenal arteries; PHA = proper hepatic arteries; SMA = superior mesenteric arteries; arcade 1 = pancreaticoduodenal artery (PDA) near the SMA; arcade 2 = mid-portion of the PDA; arcade 3 = the portion near the GDA; N/A = not available.

[a] Considered statistically significant by Mann–Whitney test.

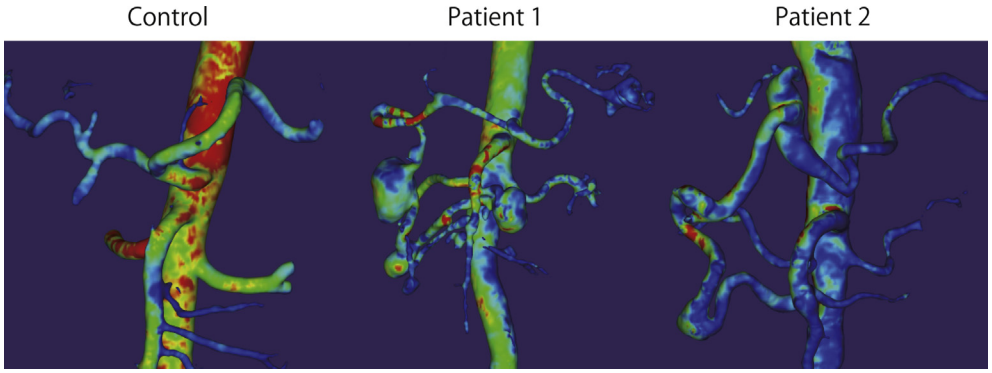

Figure 3. Three-dimensional visualization of wall shear stress (WSS) of the systolic phase in a control participant, patient 1, and patient 2. *Note*. Arterial wall color indicates WSS, i.e., the color changes from blue to red as the WSS increases. Blue indicates 0 Pa; red indicates WSS >2.0 Pa.

heterogeneous patterns of WSS, i.e., hot and cold spots of WSS distributed along the same artery, than control participants, where distribution of WSS seemed to be more homogeneous. In patients, the average value of WSS in the PDA was similar to that of other visceral arteries (Table 3). However, OSI maps, which reflect more instantaneous WSS vector fluctuation from the main stream direction, showed multiple regions with extremely high OSI values (Fig. 4; red and yellow areas represent OSI > 0.3 and 0.3 > OSI > 0.2, respectively) distributed heterogeneously throughout the PDA in all patients with PDA aneurysms. In contrast, those hot regions were rarely observed in control participants.

Flow volume and blood velocity

Tables 4 and 5 show the average volume of blood flow and flow velocity, respectively, which were obtained by 4D-Flow in the control and patient groups. Positive values indicate antegrade flow direction, while negative values indicate retrograde flow direction. The flow patterns were pulsatile; however, they were not bi- or tri-phasic; moreover, the flow direction was mostly uni-directional throughout the cardiac cycle (Supplementary Figure). In patients, both CHA and GDA had retrograde flow. Flow volume in GDA and SMA was significantly higher in patients than in control participants. Maximum flow velocity was significantly increased in GDA, but significantly decreased in SMA in patients compared with control participants.

Table 3. Wall shear stress (Pa) in control participants and patients.

	Control participants	Patients	*p*
Aorta	0.404 ± 0.150	0.413 ± 0.198	0.468
CHA	0.293 ± 0.093	0.330 ± 0.072	0.285
GDA	0.210 ± 0.071	0.517 ± 0.331	0.044[a]
PHA	0.215 ± 0.052	0.286 ± 0.212	0.377
SMA	0.338 ± 0.171	0.709 ± 0.376	0.840
Arcade 1	N/A	0.332 ± 0.216	
Arcade 2	N/A	0.297 ± 0.112	
Arcade 3	N/A	0.325 ± 0.168	
Aneurysm	N/A	0.306 ± 0.119	

Note. All data are the mean ± SD.CHA = common hepatic arteries; GDA = gastroduodenal arteries; PHA = proper hepatic arteries; SMA = superior mesenteric arteries; arcade 1 = pancreaticoduodenal artery (PDA) near the SMA; arcade 2 = mid-portion of the PDA; arcade 3 = the portion near the GDA; N/A = not available.
[a] Considered statistically significant by Mann–Whitney test.

DISCUSSION

Previous reports have shown that a considerable part of PDA aneurysms with CA occlusion/stenosis are atherosclerotic. However, the most frequent cause of CA occlusion in those cases is not the atherosclerotic degeneration itself but compression by the median arcuate ligament. Upon CA occlusion, the rich anastomotic network between the CA and the SMAs has to supply blood to the liver, stomach, and pancreas via the PDA. Previous studies have reported that hemodynamic changes are responsible for initiation, growth, and rupture of intracranial aneurysms.[15–17] In this study, we used 4D-Flow for non-invasive evaluation of hemodynamic changes in in vivo blood flow in the abdominal visceral arteries of patients with PDA aneurysms concomitant with CA occlusion. This emerging technique has previously been used for investigating hemodynamics in various anatomical locations, including the neck, brain, and thorax.[18–20]

In the present study, flow volume was increased in both GDA and SMA in patients with PDA aneurysm compared with control participants. As anticipated, both CHA and GDA showed retrograde flow in PDA patients, i.e., the direction of blood flow in CHA and GDA was from right to left, and from the caudal to cranial side, respectively. For PDA arteries, 4D-Flow could depict images of blood flow only in patients with PDA aneurysm, which suggested increased blood flow and enlargement of the PDA. However, this hindered comparison of hemodynamic changes between patients and control participants. The data we obtained regarding PDAs showed that PDA segments (arcades 1–3) had similar values of flow volume and flow velocity as observed in CHA, GDA, and PHA in control participants; this suggested that PDAs that are generally undetectable on MRI became so enlarged as to be similar to the size of major visceral arteries. The streamlines of arteries, which are instantaneously tangent to the velocity vector of blood flow, show the direction of flow at any chosen time point. The flow patterns depicted by the streamline visualization showed that enlarged PDA arteries had vortex or helical

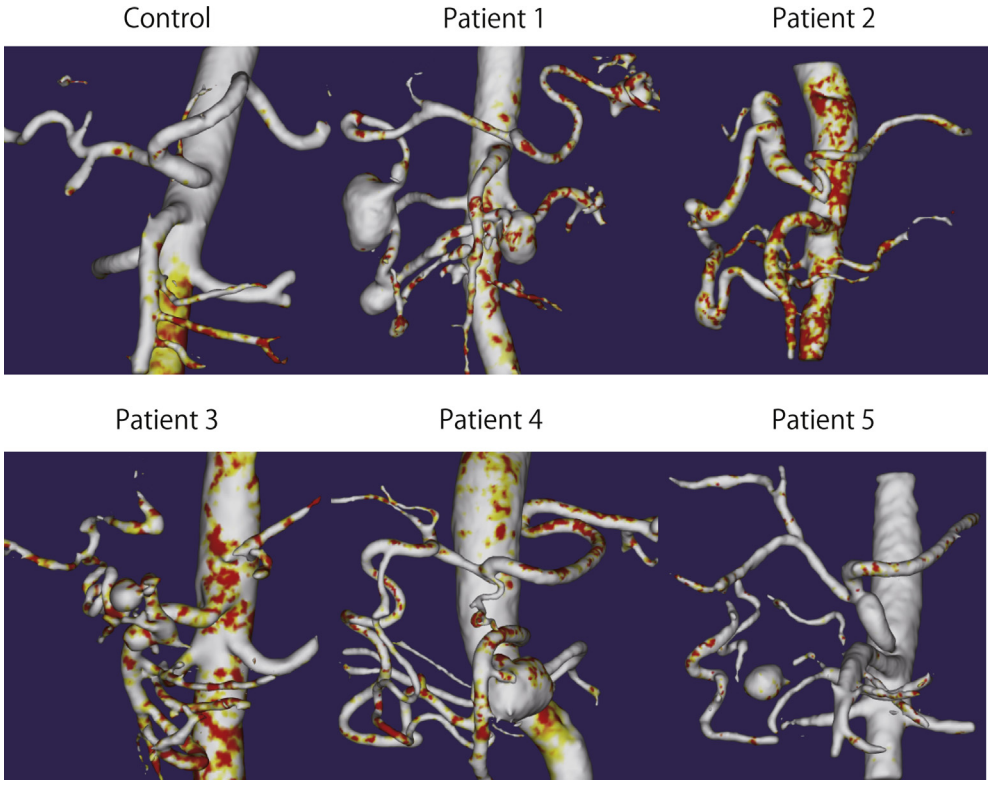

Figure 4. Three-dimensional visualization of oscillatory shear index (OSI) in a control participant and all patients with PDA aneurysm. *Note*. Color-coded images indicate distribution of OSI, i.e., the color changes from white to red as the OSI increases. White indicates OSI = 0.1; red indicates OSI >0.3.

flow patterns in all patients. Similar to other aneurysms, such as cerebral artery aneurysms or abdominal aortic aneurysms, PDA aneurysms also show vortex flow patterns in streamline images.[21,22] The temporal average over the cardiac cycle of the absolute WSS in PDA showed heterogenous distribution of low WSS area. OSI mapping identified extremely high OSI areas, which were heterogeneously distributed not only in PDA, but also in GDA and SMA. Mantha et al.[16] reported that intracranial aneurysms occur at sites with low WSS. Low WSS causes degeneration and apoptosis of endothelial cells.[23,24] Endothelial cells are very sensitive to instantaneous fluctuations of WSS;[12,25] therefore, we calculated OSI, which reflects WSS vector fluctuation from the main stream direction at the calculated point during one cardiac cycle. We, and others, have previously reported that low WSS and high OSI are important factors contributing to rupture of intracranial aneurysms.[22,26] Both low WSS and high OSI also cause intimal hyperplasia and accelerate atherosclerosis progression.[23,27] Indeed, in this study, all PDA aneurysms subjected to histological analysis were atherosclerotic. Considering these

Table 4. Flow volume (mm^3/s) in control participants and patients.

	Control participants	Patients	*p*
Aorta	35,913.5 ± 8892.5	37,314.8 ± 9195.7	0.468
CHA	492.2 ± 371.7	−1306.8 ± 1397.6	0.093[a]
GDA	286.6 ± 217.5	−1742.2 ± 960.6	0.044[a]
PHA	213.5 ± 235.6	394.9 ± 930.1	0.232
SMA	2337.6 ± 1131.7	2539.8 ± 4012.1	0.031[a]
Arcade 1	N/A	1251.8 ± 1895.7	
Arcade 2	N/A	368.7 ± 498.7	
Arcade 3	N/A	547.3 ± 596.6	

Note. All data are the mean ± SD. Positive values of flow volume indicate antegrade flow direction, while negative values indicate retrograde flow direction.CHA = common hepatic arteries; GDA = gastroduodenal arteries; PHA = proper hepatic arteries; SMA = superior mesenteric arteries; arcade 1 = pancreaticoduodenal artery (PDA) near the SMA; arcade 2 = mid-portion of the PDA; arcade 3 = the portion near the GDA; N/A = not available.

[a] Considered statistically significant by Mann–Whitney test.

Table 5. Maximum blood velocity (mm/s) in control participants and patients.

	Controls	Patients	*p*
Aorta	207.8 ± 75.7	207.0 ± 71.7	0.468
CHA	62.1 ± 30.5	−68.6 ± 79.5	0.093
GDA	52.7 ± 19.8	−156.4 ± 97.2	0.044[a]
PHA	41.6 ± 30.0	33.1 ± 110.3	0.146
SMA	134.3 ± 70.9	67.0 ± 269.7	0.031[a]
Arcade 1	N/A	83.9 ± 119.7	
Arcade 2	N/A	25.3 ± 71.5	
Arcade 3	N/A	76.9 ± 72.3	

Note. All data are the mean ± SD. Positive values of maximum blood velocity indicate antegrade flow direction, while negative values indicate retrograde flow direction.CHA = common hepatic arteries; GDA = gastroduodenal arteries; PHA = proper hepatic arteries; SMA = superior mesenteric arteries; arcade 1 = pancreaticoduodenal artery (PDA) near the SMA; arcade 2 = mid-portion of the PDA; arcade 3, = the portion near the GDA; N/A = not available.

[a] Considered statistically significant by Mann–Whitney test.

findings, we speculate that aneurysmal formation in PDA region is associated with secondary hemodynamic changes due to CA occlusion. To confirm our hypothesis, a prospective study should be performed to observe patients with CA occlusion using 4D-Flow and periodical follow-up of the PDA. However, it may be difficult to recruit a large number of patients who agree to undergo periodical 4D-Flow study.

In this study, use of 4D-Flow provided new insights into the hemodynamic changes in CA occlusion. As we discussed earlier, 4D-Flow identified retrograde flow of CHA and GDA in patients with PDA aneurysm who had concomitant CA occlusion. The method also proved its potential to be used as a preoperative indicator of blood flow in PDA. Pancreaticoduodenectomy involves sacrifice of the GDA; this poses an ischemic threat to the liver, stomach, pancreas, and various anastomoses in patients with CA occlusion. In such cases, aorto-hepatic bypass or preservation of GDA should be considered to avoid ischemia.[28] However, in case of CA stenosis, preoperative information on which artery (either CA or GDA) is dominant in supplying blood to the liver is important to perform pancreaticoduodenectomy safely. Nowadays, the right gastroepiploic artery is often used as a bypass conduit for coronary artery bypass grafting.[29,30] Therefore, preoperative understanding of hemodynamics in the PDA region is important in hepato-pancreato-biliary surgery. Utilization of 4D-Flow for patients who need pancreaticoduodenectomy may help surgeons in operative planning.

In conclusion, 4D-Flow identified hemodynamic changes in the PDA in patients with PDA aneurysms concomitant with CA occlusion. In patients with CA occlusion, both CHA and GDA showed retrograde flow. PDAs had increased blood flow with heterogeneous distribution of low WSS and high OSI areas. These changes may be associated with atherosclerotic tissue degeneration and formation of atherosclerotic aneurysms.

CONFLICTS OF INTEREST

Toshiyasu Shimizu is an employee of Renaissance Technology Inc., which produces the flow analysis software used in this study. Tetsuya Wakayama is an employee of GE Healthcare Japan, which is the vendor of the MR system used in this study. The remaining authors have no conflicts of interest to declare.

FUNDING

None.

APPENDIX A. SUPPLEMENTARY DATA

Supplementary data related to this article can be found online at http://dx.doi.org/10.1016/j.ejvs.2013.06.011.

REFERENCES

1 Stanley JC, Wakefield TW, Graham LM, Whitehouse Jr WM, Zelenock GB, Lindenauer SM. Clinical importance and management of splanchnic artery aneurysms. *J Vasc Surg* 1986;**3**(5):836—40.
2 de Perrot M, Berney T, Deléaval J, Bühler L, Mentha G, Morel P. Management of true aneurysms of the pancreaticoduodenal arteries. *Ann Surg* 1999;**229**(3):416—20.
3 Uher P, Nyman U, Ivancev K, Lindh M. Aneurysms of the pancreaticoduodenal artery associated with occlusion of the celiac artery. *Abdom Imaging* 1995;**20**(5):470—3.
4 Sugiyama K, Takehara Y. Analysis of five cases of splanchnic artery aneurysm associated with coeliac artery stenosis due to compression by the median arcuate ligament. *Clin Radiol* 2007;**62**:688—93.
5 Wigstrom L, Sjoqvist L, Wranne B. Temporally resolved 3D phase-contrast imaging. *Magn Reson Med* 1996;**36**(5):800—3.
6 Bogren HG, Buonocore MH. 4D magnetic resonance velocity mapping of blood flow patterns in the aorta in young vs. elderly normal subjects. *J Magn Reson Imaging* 1999;**10**(5):861—9.
7 Geiger J, Markl M, Herzer L, Hirtler D, Loeffelbein F, Stiller B, et al. Aortic flow patterns in patients with Marfan syndrome assessed by flow-sensitive four-dimensional MRI. *J Magn Reson Imaging* 2012;**35**(3):594—600.
8 Liu Z, Moorhead 2nd RJ, Groner J. An advanced evenly-spaced streamline placement algorithm. *IEEE Trans Vis Comput Graph* 2006;**12**(5):965—72.
9 Masaryk AM, Frayne R, Unal O, Krupinski E, Strother CM. In vitro and in vivo comparison of three MR measurement methods for calculating vascular shear stress in the internal carotid artery. *AJNR* 1999;**20**(2):237—45.
10 Cheng CP, Parker D, Taylor CA. Quantification of wall shear stress in large blood vessels using Lagrangian interpolation functions with cine phase-contrast magnetic resonance imaging. *Ann Biomed Eng* 2002;**30**(8):1020—32.
11 Isoda H, Ohkura Y, Kosugi T, Hirano M, Alley MT, Bammer R. Comparison of hemodynamics of intracranial aneurysms between MR fluid dynamics using 3D cine phase-contrast MRI and MR-based computational fluid dynamics. *Neuroradiology* 2010;**52**(10):913—20.
12 He X, Ku DN. Pulsatile flow in the human left coronary artery bifurcation: average conditions. *J Biomech Eng* 1996;**118**(1):74—82.
13 Cohen J. A coefficient of agreement for nominal scales. *Educ Psychol Meas* 1960;**20**(1):37—46.
14 Landis JR, Koch GG. The measurement of observer agreement for categorical data. *Biometrics* 1977;**33**(1):159—74.
15 Imbesi SG, Kerber CW. Why do ulcerated atherosclerotic carotid artery plaques embolize? A flow dynamics study. *Am J Neuroradiol* 1998;**19**(4):761—6.
16 Mantha A, Karmonik C, Benndorf G, Storther C, Metcalfe R. Hemodynamics in a cerebral artery before and after the formation of an aneurysm. *Am J Neuroradiol* 2006;**27**(5):1113—8.
17 Meng H, Wang Z, Hoi Y, Gao L, Metaxa E, Swartz DD, et al. Complex hemodynamics at the apex of an arterial bifurcation induces vascular remodeling resembling cerebral aneurysm initiation. *Stroke* 2007;**38**(6):1924—31.
18 Markl M, Kilner PJ, Ebbers T. Comprehensive 4D velocity mapping of the heart and great vessels by cardiovascular magnetic resonance. *J Cardiovasc Magn Reson* 2011;**13**:7.
19 Barker AJ, Markl M, Bürk J, Lorenz R, Bock J, Bauer S, et al. Bicuspid aortic valve is associated with altered wall shear stress in the ascending aorta. *Circ Cardiovasc Imaging* 2012;**5**(4):457—66.
20 Hsiao A, Lustig M, Alley MT, Murphy MJ, Vasanawala SS. Evaluation of valvular insufficiency and shunts with parallel-imaging compressed-sensing 4D phase-contrast MR imaging with stereoscopic 3D velocity-fusion volume-rendered visualization. *Radiology* 2012;**265**(1):87—95.

21 Fatouraee N, Amini AA. Regularization of flow streamlines in multislice phase-contrast MR imaging. *IEEE Trans Med Imaging* 2003;**22**(6):699—709.
22 Isoda H, Ohkura Y, Kosugi T, Hirano M, Takeda H, Hiramatsu H, et al. In vivo hemodynamic analysis of intracranial aneurysms obtained by magnetic resonance fluid dynamics (MRFD) based on time-resolved three-dimensional phase-contrast MRI. *Neuroradiology* 2010;**52**(10):921—8.
23 Malek AM, Alper SL, Izumo S. Hemodynamic shear stress and its role in atherosclerosis. *J Am Med Assoc* 1999;**282**(21): 2035—42.
24 Sho E, Sho M, Singh TM, Xu C, Zarins CK, Masuda H. Blood flow decrease induces apoptosis of endothelial cells in previously dilated arteries resulting from chronic high blood flow. *Arterioscler Thromb Vasc Biol* 2001;**21**(7):1139—45.
25 Ku DN, Giddens DP, Zarins CK, Glagov S. Pulsatile flow and atherosclerosis in the human carotid bifurcation. Positive correlation between plaque location and low oscillating shear stress. *Arteriosclerosis* 1985;**5**(3):293—302.
26 Kawaguchi T, Nishimura S, Kanamori M, Takazawa H, Omodaka S, Sato K, et al. Distinctive flow pattern of wall shear stress and oscillatory shear index: similarity and dissimilarity in ruptured and unruptured cerebral aneurysm blebs. *J Neurosurg* 2012;**117**:774—80.
27 Friedman MH, Hutchins GM, Bargeron CB, Deters OJ, Mark FF. Correlation between intimal thickness and fluid shear in human arteries. *Atherosclerosis* 1981;**39**(3):425—36.
28 Nagai H, Ohki J, Kondo Y, Yasuda T, Kasahara K, Kanazawa K. Pancreatoduodenectomy with preservation of the pylorus and gastroduodenal artery. *Ann Surg* 1996;**223**(2):194—8.
29 Suma H, Fukumoto H, Takeuchi A. Coronary artery bypass grafting by utilizing in situ right gastroepiploic artery: basic study and clinical application. *Ann Thorac Surg* 1987;**44**(4): 394—7.
30 Nakamura N, Irie T, Ochiai T, Kudo A, Itoh K, Tanaka S. Pancreatoduodenectomy after coronary artery bypass grafting using the right gastroepiploic artery: a case report. *Hepatogastroenterology* 2011;**58**(109):1137—41.